Modeling Charge Resonance in Cationic Molecular Clusters: Combining DFT-Tight Binding with Configuration Interaction

Mathias Rapacioli, Fernand Spiegelman, Anthony Scemama, André Mirtschink

Modeling charge resonance in ionized molecular clusters: combining DFT-Tight Binding with configuration interaction

Mathias Rapacioli,* Fernand Spiegelman, Anthony Scemama, and André Mirtschink

1-Université de Toulouse, UPS, LCPQ (Laboratoire de Chimie et Physique Quantiques), IRSAMC, 118 Route de Narbonne, F-31062 Toulouse, France

2-CNRS, LCPQ (Laboratoire de Chimie et Physique Quantiques), IRSAMC, F-31062 Toulouse

E-mail: mathias.rapacioli@irsamc.ups-tlse.fr

Abstract

Recently, Wu *et al.*[1] proposed to investigate charge resonance situations in molecular complexes via a method expressing Configuration Interaction (CI) in a valence bond-like based multi-configurational basis determined from constrained DFT calculations. We adapt this method within the Self-Consistent Charge Density Functional Tight Binding (SCC-DFTB) approach and provide the expressions for the gradient of the energy with respect to the nuclear coordinates, allowing for full structural optimization. The method is shown to correct for the wrong SCC-DFTB behavior of the potential energy surface in the dissociation regions. We apply this scheme to determine the structural and stability properties of some positively charged molecular dimers, respectively the benzene dimer cation and the water dimer cation. The method is shown to yield binding energies in good agreement with experimental data and high level reference calculations.

*To whom correspondence should be addressed

1 Introduction

The description of molecular clusters requires to take into account the various contributions of the intermolecular energy, including the Pauli repulsion, the Coulomb interaction, and the London dispersion. The description of the electronic structure of singly ionized molecular clusters requires to consider two further essential contributions, the first one being charge resonance which may cause the charge to be partially or totally delocalized over the molecular units, the second one being the polarization contribution due to the influence of the charge. Both of them yield a stabilization of the charged species as compared to the analogous neutrals. A proper description requires correct balance between charge delocalization and polarization forces.

While Density Functional Theory (DFT) is an appealing method to describe the electronic properties of clusters up to a few tenths, maybe a few hundreds atoms, at least in single point calculations, the use of the most common functionals is known to fail to describe properly dispersion forces. This is a first handicap to deal with molecular clusters. Search for new functionals accounting for dispersion[2–10] is a very active field, while semi-empirical corrections to standard DFT calculations are also used[11–18]. Description of charge resonance in molecular clusters is another serious problem in standard Density Functional approaches. Using canonical Kohn-Sham orbitals, one arising problem is the self-interaction of the delocalized charge. This aspect is particularly prevalent at dissociation, for instance in a cationic molecular complex involving two identical units, and which should dissociate into one molecular cation and one neutral, whereas in restricted scheme DFT the charge is asymptotically equally shared by the two units, breaking the energy additivity and further introducing a spurious Coulomb interaction between the two moieties. Although such an artifact is essential at the dissociation, it is also expected to play a role all over the potential energy surface, including the equilibrium geometries.

A correct description of dissociation is in principle easily obtained if one uses a multiconfigurational nature of the wave function. This can be achieved by high level methods like Configuration Interaction (CI) based methods (Multi-Configurational Self-Consistent Field MCSCF, Multi-Rereference Configuration Interaction MRCI) or Coupled Cluster approaches but at a high

computational price. Such calculations may provide benchmarks on reasonably small systems (essentially dimers) but rapidly exceed today's possibilities as soon as the molecular units exceed a few tens of atoms.

One of the tracks to circumvent the drawbacks of present state DFT in an *ab initio* framework is to combine CI for describing long range (lr) electron-electron interactions and DFT for the short range electron-electron interactions (sr). This gave rise to the lr-sr formalism following Savin's formulation,[19–22] which make possible combinations of MP2, Coupled Cluster and/or CI approaches with Density Functional Theory, via a partition of the electron-electron Coulomb interaction. This formulation is quite attractive, nevertheless its numerical cost is significantly larger than that of a standard DFT calculation.

On the other hand, charge resonance (or excitation resonance) appears quite simply in valence bond-like approaches[23–26] explicitely taking into account the multiconfigurational nature of the wavefunction via the definition of a basis in which charge (or excitation) is localized on a given fragment of the system. This is the essence of the excitonic models originating from solid states, but also used in molecular materials and even biological systems. An application to molecular cluster cations and in particular polycyclic aromatic hydrocarbon (PAH) cluster cations was published by Bouvier *et al.*[27] defining a resonance charge model based on frozen molecules, and parametrized from *ab initio* CI calculations of dimers. Diatomics-In-Molecule modeling of singly ionized rare gas clusters can also be expressed in valence bond picture in a basis of atom-localized hole configurations with no internal geometrical structure,[**? ?**] paving the way for extensive simulations of the electronic and dynamical properties of ionized rare gas clusters (see for instance **? ?**

.

More recently, the concept of using a valence bond configuration description combined with a DFT framework was proposed by the group of Van Voorhis *et al.*[1,28–30] to investigate charge delocalization in mixed valence compounds exhibiting possible bi-stability with the perspective of controlling charge transfer. They developed a method combining constrained DFT with a small CI-like scheme (CDFT-CI) to deal with charge delocalization in extended systems. This is extremely

appealing from the computational point of view, since the size of the CI increases linearly with the number of fragments, and not as a power of the total number of active electrons in the whole system, which is a bottleneck. The Self-Consistent-Charge Density Functional based Tight Binding (SCC-DFTB)[31–34] is an alternative to DFT in the quest of addressing large systems. It is derived from DFT through several approximations allowing the use of parametrized tables to avoid the explicit calculation of overlap and interaction integrals. As SCC-DFTB is derived from DFT it also inherits its lack in describing charge resonance. Recently, we presented a preliminary transcription of the CDFT-CI method in SCC-DFTB framework using also approximations to determine the CI couplings. We provided applications to coronene clusters with constrained geometries, because of lack of the gradient[35].

In the present paper, we present the general adaptation of the CDFT+CI method to the SCC-DFTB framework, with the aim of future investigations of charge resonance in molecular clusters with either large units or large size. This method is called the DFTB-VBCI (Valence Bond CI). In order to perform geometry optimization, we also derive analytical expressions for the energy gradient with respect to the nuclear coordinates, which we use to achieve full structural optimization for the benzene dimer and water dimer cations, respectively.

Section 2 is devoted to the presentation of the general methodology and the DFTB-VBCI approach and the derivation of analytical expressions for the nuclear forces. In section Section 3, we benchmark the method on benzene and water ionic dimers on the basis of comparisons with high level calculations. Outlines and perspectives are given in section Section 4.

2 Methodology

The DFTB-VBCI method is an adaptation of the DFT+CI approach[1,28–30] to the SCC-DFTB scheme with the focus on treating charge resonance in ionized molecular clusters. In that approach, the wave function of the system Ψ is decomposed on a basis $\{\Phi^I\}$ of configurations where the charge is localized on different fragments of the system. The intuitive decomposition of a

molecular cluster leads to identify each of the N_{frag} monomers to a fragment and the wave function becomes

$$\Psi = \sum_{I}^{N_{\text{frag}}} b_I \Phi^I \tag{1}$$

where Φ^I is the configuration where the charge is fully carried by fragment I. Each charge localized configuration Φ^I is a single Slater determinant, built from the molecular orbitals (MO) $\{\phi_i^I\}$ resulting from a constrained SCC-DFTB calculation. These VB like configurations then interact within a small CI-like scheme giving their coefficients b_I in the wave function and the ground state energy.

In this methodological part, we first briefly recall the SCC-DFTB scheme basics (Section 2.1) before explaining the derivation of the charge localized configurations Φ^I using the constrained SCC-DFTB (Section 2.2) and the CI-like scheme calculation (Section 2.3). We present then analytical expressions for the nuclear forces (Section 2.4) and some further approximations to accelerate the approach (Section 2.5). We adopt different font conventions to distinguish between matrices expressed on different basis sets. For instance, the Hamiltonian matrix is written as H in the atomic orbital (AO) basis set; $\mathscr{H}$ in the molecular orbital (MO) basis set and $\mathbf{H}$ in the determinant basis set (the basis of the charge-localized configurations.

2.1 DFT and SCC-DFTB

Several reviews on the DFTB and SCC-DFTB method can be found in the litterature.[31–34] The SCC-DFTB differs from the DFT expressed on a local basis set by the following approximations: (i) the DFT energy is expanded up to the second order with respect to charge density fluctuations around a given reference density (ii) all three center interaction integrals are neglected (iii) the MO are expressed in a minimal atomic basis set

$$\phi_i = \sum_{\mu} c_{i\mu} \varphi_\mu \tag{2}$$

(iv) the short distance repulsive potential is expressed as a function of two body interactions (v) the second order term in the DFT energy expansion is expressed as a function of atomic Mulliken charges and a Γ matrix. With these approximations, the total SCC-DFTB energy reads

$$E^{\mathrm{SCC-DFTB}} = \sum_{\alpha,\beta\neq\alpha}^{\mathrm{atoms}} E^{\mathrm{rep}}_{\alpha\beta} + \sum_i n_i \langle\phi_i|\hat{H}^0|\phi_i\rangle + \frac{1}{2}\sum_{\alpha,\beta}^{\mathrm{atoms}} \Gamma_{\alpha\beta} q_\alpha q_\beta \tag{3}$$

where $\hat{H}^0$ is the Kohn-Sham operator at the reference density and $E^{\mathrm{rep}}_{\alpha\beta}$ is the repulsive potential between atoms α and β. The matrix elements of H^0 are expressed in the atomic basis set, $\Gamma_{\alpha\beta}$ and $E^{\mathrm{rep}}_{\alpha\beta}$ are interpolated from two body DFT calculations. n_i are the atomic orbital occupation numbers and q_α are the atomic Mulliken charges. The energy minimization is obtained by solving self-consistently the secular equation

$$\sum_\nu c_{i\nu}(H_{\mu\nu} - \varepsilon_i S_{\mu\nu}) = 0 \ \ \forall \mu, i \tag{4}$$

S is the atomic basis overlap matrix and the Hamiltonian matrix reads $H = H^0 + H^1$ with

$$H^1_{\mu\in\alpha;\nu\in\beta} = \frac{1}{2} S_{\mu\nu} \sum_\xi^{\mathrm{atoms}} (\Gamma_{\alpha\xi} + \Gamma_{\xi\beta}) q_\xi \tag{5}$$

where $\mu \in \alpha$ means that the atomic orbital μ belongs to atom α.

2.2 Constrained SCC-DFTB

Similarly to the constrained DFT[28], the MOs $\{\phi_i^I\}$, used to build the configuration Φ^I, are obtained from a minimization of the SCC-DFTB energy with the constraints that the charge is carried by fragment I and that the orbitals are orthonormalized. The corresponding Lagrangian is

$$\mathscr{L} = E^{\mathrm{SCC-DFTB}}(\{\phi_i^I\}) + \sum_{ij} \Lambda^I_{ij} \left(\langle\phi_i^I|\phi_j^I\rangle - \delta_{ij}\right) + V^I \left(\sum_i n_i \langle\phi_i^I|\hat{P}^I|\phi_i^I\rangle - N^I\right) \tag{6}$$

where V^I is the Lagrange multiplier ensuring the charge localization constraint, $\hat{P}^I$ is the projector of the density on fragment I, N^I is the number of electrons on fragment I which defines the charge localization, Λ_{ij} are the Lagrange multipliers ensuring the orbitals orthonormality constraint. Wu and Van VoorhisWu and Van Voorhis[28] discussed the effect of several localizations, based on different charge definitions (Mulliken, Boys, Löwdin), on the constrained energy and finally adopting the Löwdin approach. We used for the constrained SCC-DFTB the Mulliken charge definition because (i) the defects of Mulliken charges are less crucial than in DFT due to the use of a minimal atomic basis set (no diffuse functions) and (ii) in the mostly used version, SCC-DFTB is a Mulliken charge based approach and all the matrix elements have been parametrized for this charge defintion. This choice leads to the expression for the constraint

$$\sum_{i\nu\mu} n_i c^I_{i\nu} c^I_{i\mu} P^I_{\nu\mu} = N^I \tag{7}$$

P^I being the projection matrix expressed as[28]

$$P^I_{\mu\nu} = \begin{cases} 0 \text{ if } \mu \notin I \text{ and } \nu \notin I \\ S_{\mu\nu} \text{ if both } \mu \in I \text{ and } \nu \in I \\ \frac{1}{2} S_{\mu\nu} \text{ for other cases } (\mu \in I \text{ or } \nu \in I) \end{cases}$$

The secular equation (Eq. (4)) should now be solved with the H matrix modified as follows

$$H_{\mu\nu} = H^0_{\mu\nu} + H^1_{\mu\nu} + V^I P^I_{\mu\nu}$$

Similarly to the constrained DFT, Eq. (4) must now be solved self-consistently over the atomic charges and contains an unknown Lagrange multiplier V^I. To overcome some convergence problems, we have implemented three ways of solving this equation which can be used alternatively until one of them converges.

-i- The first one (similar to that of[36]) consists in solving the secular equation with an inner loop

to calulate the V^I Lagrange multiplier satisfying the constraint keeping fixed charges q_α in the Hamiltonian. An external loop over the Mulliken charges is performed to reach a self-consistent solution.

-ii- The second approach consists in inverting the two previous loops, i.e. the inner loop ensuring the self-consistence over the Mulliken charges and the external loop allowing the determination of the Lagrange multiplier V^I.

-iii- The third approach is somewhat different and consists in three steps. First, a MO guess is generated for isolated fragments. The full set of MOs is is orthonormalized with a Löwdin procedure. These MOs do not correspond to an energy minimum and do not satisfy the charge localization constraint. In the second step, the MOs evolve to change the number of electrons on fragment I with the iterative procedure

$$\phi_i^I(n+1) = \phi_i^I(n) + \alpha \left(p^I \phi_i^I(n) + \sum_j \phi_j^I(n) \Lambda_{ij} \right) \quad \forall i \tag{8}$$

where n is the iteration step. The third term ensures the orthonormalization constraint. Transposing this equation in the atomic basis set gives the evolution of the MOs

$$C^I(n+1) = C^I(n) + \alpha (S^{-1} P^I C^I(n) + X C^I(n)) \tag{9}$$

where $X = \alpha S^{-1} \Lambda$. At each step, the α coefficient is adapted to increase or decrease the number of electrons on fragment I and the X matrix is calculated solving a second order equation equivalent to the Rickaert[37] algorithm already implemented for SCC-DFTB Car Parrinello molecular dynamics[38]. Once a solution satisfying the density constraint is achieved, the last step consists in relaxing the MO to minimize the energy, conserving the charge localization and orthonormality constraints

$$\phi_i^I(n+1) = \phi_i^I(n) + \alpha \left(\frac{dE}{d\phi_i^{I*}} + \sum_j \phi_j^I \Lambda_{ij} + V^I P^I \phi_i^I \right) \tag{10}$$

giving the evolution of the coefficients

$$C^I(n+1) = C^I(n) + \alpha(S^{-1}HC^I(n) + XC^I(n) + V^I S^{-1} P^I C^I(n)) \tag{11}$$

This step requires both the calculation of X and V^I. Starting from a given V^I (the one of the previous step if $n > 1$), $C^I(n+1)$ is determined, calculating X with the Rickaert algorithm. The charge carried by fragment I with these new coefficients is calculated. If this charge is too large (resp. too small), V^I is decreased (resp. increased). The process is repeated until the molecular charge satisfies the constraint. Finally, the MOs converge to the the charge-localized solution.

2.3 The Configuration Interaction-like scheme

The set of MO $\{\phi_i^I\}$ obtained from a constrained SCC-DFTB is used to build the charge-localized configurations Φ^I as single Slater determinants. The coefficients b_I of these configurations in the total wave function Ψ (see Eq. (1)) are obtained by solving the CI-like scheme

$$\begin{pmatrix} \mathbf{H}_{11} & \mathbf{H}_{12} & .. & \mathbf{H}_{1n} \\ \mathbf{H}_{21} & \mathbf{H}_{22} & .. & \mathbf{H}_{2n} \\ : & : & :: & : \\ \mathbf{H}_{n1} & . & .. & \mathbf{H}_{nn} \end{pmatrix} \begin{pmatrix} b_1 \\ b_2 \\ : \\ b_n \end{pmatrix} = E \begin{pmatrix} \mathbf{S}_1 & \mathbf{S}_{12} & .. & \mathbf{S}_{1n} \\ \mathbf{S}_{21} & \mathbf{S}_2 & .. & \mathbf{S}_{2n} \\ : & : & :: & : \\ \mathbf{S}_{n1} & . & .. & \mathbf{S}_{nn} \end{pmatrix} \begin{pmatrix} b_1 \\ b_2 \\ : \\ b_n \end{pmatrix} \tag{12}$$

where $\mathbf{S}_{IJ}$ is the two configurations overlap $\langle \Phi^I | \Phi^J \rangle$ and $\mathbf{H}_{II}$ is the energy of the configuration Φ^I already calculated with the constrained SCC-DFTB. Following the approach of Wu *et al.*[1,29], the coupling elements $\mathbf{H}_{IJ}$ are calculated by

$$\mathbf{H}_{IJ} = \frac{1}{2}(\mathbf{H}_{II} + \mathbf{H}_{JJ} + N^I V^I + N^J V^J)\mathbf{S}_{IJ} - \frac{1}{2}(V^I \langle \Phi^I | \hat{P}^I | \Phi^J \rangle + V^J \langle \Phi^I | \hat{P}^J | \Phi^J \rangle) \tag{13}$$

In the case of degenerate systems, one can also include more than one configuration to represent the charge localization on a given fragment, as it will be shown in the applications of Section 2.4.

Solving Eq. (12) provides both the ground state of the system and some excited states generated via charge resonance. Although these excited states are of interest, for instance in spectroscopy, we focus in this work on the ground state which corresponds to the lowest eigenvalue E_g.

2.4 Analytical gradient

Calculating derivatives of the energy upon atomic nuclei is required to perform molecular dynamics or geometry optimization. Their numerical calculation is possible by finite differences but the number of energy calculations $(2 \times 3N_{\text{atoms}})$ turns out to be quite large even for small systems. In SCC-DFTB, it is convenient to use the derivatives of the matrix elements (H^0, S, Γ) which are known and tabulated. Differentiating Eq. (12) with respect to the nuclear coordinate $\vec{R}_a$ of atom a leads to the force expression

$$\vec{\nabla}_a E_g = \sum_{IJ} b_I b_J \left(\vec{\nabla}_a \mathbf{H}_{IJ} - E_g \vec{\nabla}_a \mathbf{S}_{IJ} \right) \tag{14}$$

We now present the calculation of the derivatives for the diagonal and off-diagonal elements separately. The differentiation operator $\vec{\nabla}_a$ is replaced by the symbol ∂_a to simplify the expressions.

2.4.1 Derivative of the diagonal element

The diagonal element $\mathbf{H}_{II}$ is the energy of the configuration Φ^I. Differentiating (Eq. Eq. (3)) and using the eigenvalue equation (Eq. (4)), the molecular charge conservation (Eq. (7)) and orthonormality constraints leads to the analytical

$$\partial_a \mathbf{H}_{II} = \partial_a E^{\text{rep}} + \sum_i n_i \sum_{\mu\nu} c_{i\nu} c_{i\mu} \left(\partial_a H^0_{\mu\nu} + V^I \partial_a P^I_{\mu\nu} + (\frac{H^1_{\mu\nu}}{S_{\mu\nu}} - \varepsilon_i) \partial_a S_{\mu\nu} \right) + q_a \sum_b \partial_a \Gamma_{ab} q_b \tag{15}$$

2.4.2 Derivative of the off-diagonal elements

The differentiation of the off-diagonal elements is obtained by differentiating Eq. (13) to give

$$\partial_a \mathbf{H}_{IJ;I\neq J} = \frac{1}{2}A_{IJ} + \frac{1}{2}A_{JI}$$

with

$$\begin{aligned} A_{IJ} &= (\partial_a \mathbf{H}_{II} + N^I \partial_a V^I)\mathbf{S}_{IJ} + (\mathbf{H}_{II} + N^I V^I)\partial_a \mathbf{S}_{IJ} \\ &\quad -\langle \Phi^I | P^I | \Phi^J \rangle \partial_a V^I - V^I \partial_a \left(\langle \Phi^I | P^I | \Phi^J \rangle \right) \end{aligned} \tag{16}$$

We must now express the derivatives of the Lagrange multipliers $\partial_a V^I$ and $\partial_a V^J$, as well as the overlaps (real overlap and through the projectors) between Φ^I and Φ^J. As there is no relationship between the MO of the two configurations, there is no Hellman-Feynman type simplification for the derivatives of their overlaps. The derivatives of the orbital coefficients and of the Lagrange multipliers must be explicitely calculated. The calculation of the derivatives of the coefficients has already been expressed for DFT (see for instance[39]) and its expression only differs here through the term containing the constraint.

For a given configuration Φ^I, the derivative of the coefficients of the orbitals $\{\phi_i^I\}$ can be related to the orbitals themselves by a u matrix

$$\partial_a c_{i\mu}^I = \sum_k c_{k\mu}^I u_{ik} \tag{17}$$

The conservation of normalized MO already imposes the form of the diagonal term of the u matrix

$$u_{ii} = -\frac{1}{2}\sum_{\mu\nu} c_{i\mu}^I c_{i\nu}^I \partial_a S_{\mu\nu}. \tag{18}$$

For the off-diagonal elements $u_{ij;i\neq j}$, differentiating Eq. (4) leads to

$$u_{ij} = \frac{\partial_a \mathscr{H}_{ij} - \varepsilon_j \partial_a \mathscr{S}_{ij}}{\varepsilon_j - \varepsilon_i} \tag{19}$$

where $\partial_a \mathscr{S}$ and $\partial_a \mathscr{H}$ are the derivatives of the SCC-DFTB overlap and Hamiltonian matrices expressed in the molecular orbital basis set

$$\begin{aligned} \partial_a \mathscr{S}_{ij} &= \sum_{\mu\nu} c^I_{i\mu} c^I_{j\nu} \partial_a S_{\mu\nu} \\ \partial_a \mathscr{H}_{ij} &= \sum_{\mu\nu} c^I_{i\mu} c^I_{j\nu} \partial_a H_{\mu\nu} \end{aligned} \tag{20}$$

In the constrained SCC-DFTB, the Hamiltonian matrix derivative depends -i- on the derivatives of matrices H^0, S, Γ and P -ii- on the derivatives of the coefficients and -iii- on the derivatives of the Lagrange multipliers. These three contributions are now explicitely separated

$$\partial_a \mathscr{H}_{ij} = \partial_a \mathscr{F}_{ij} + \sum_{kl} \mathscr{A}_{ij,kl} u_{kl} + \partial_a V^I \mathscr{P}_{ij} \tag{21}$$

where $\partial_a \mathscr{F}_{ij}$ contains the first contribution

$$\partial_a \mathscr{F}_{ij} = \sum_{\mu\nu} c^I_{i\mu} c^I_{j\nu} \partial_a F \mu\nu \tag{22}$$

with

$$\begin{aligned} \partial_a F_{\mu\in\alpha,\nu\in\beta} &= \partial_a H^0_{\mu\nu} + V^I \partial_a P_{\mu\nu} + \partial_a S_{\mu\nu} \frac{H^1_{\mu\nu}}{S_{\mu\nu}} \\ &+ \tfrac{1}{2} S_{\mu\nu} \textstyle\sum_\xi \left((\partial_a \Gamma_{\alpha\xi} + \partial_a \Gamma_{\xi\beta}) q_\xi + \sum_i n_i \sum_l \sum_{\omega\in\xi} (\Gamma_{\alpha\xi} + \Gamma_{\xi\beta}) c_{i\omega} c_{il} \partial_a S_{\omega l} \right) \end{aligned}$$

The second term in Eq. (21) accounts for the Hamiltonian dependences on the orbital coefficients with

$$\mathscr{A}_{ij,kl} = \sum_{\mu\nu} c^I_{i\mu} c^I_{j\nu} \sum_\omega \frac{\partial H_{\mu\nu}}{\partial c^I_{k\omega}} c^I_{l\omega} \tag{23}$$

and

$$\frac{\partial H_{\mu\nu}}{\partial c^I_{k\omega}} = \frac{1}{2} n_k S_{\mu\nu} \sum_\xi \sum_{\lambda\in\xi} S_{\lambda\omega} (\Gamma_{\alpha\gamma} + \Gamma_{\beta\gamma} + \Gamma_{\alpha\xi} + \Gamma_{\beta\xi}) c^I_{k\lambda} \tag{24}$$

where $\mu \in \alpha; \nu \in \beta; \omega \in \gamma$. In the last term of Eq. (21), $\mathscr{P}_{ij}$ accounts for the Hamiltonian differ-

entiation upon the Lagrange multiplier

$$\mathscr{P}_{ij} = \sum_{\mu\nu} c^I_{i\mu} c^I_{j\nu} P_{\mu\nu} \tag{25}$$

Compacting the ij indices in a single m indice and the kl indices in a single n indice, we now define

$$\begin{aligned} u_m &= u_{ij} \\ v_m &= \frac{\partial_a \mathscr{F}_{ij} - \varepsilon_j \partial_a \mathscr{S}_{ij}}{\varepsilon_j - \varepsilon_i} \\ B_{mn} &= \frac{A_{ij,kl}}{\varepsilon_j - \varepsilon_i} \\ w_m &= \frac{\mathscr{P}_{ij}}{\varepsilon_j - \varepsilon_i} \end{aligned}$$

and rewrite Eq. (19)

$$\begin{aligned} u &= Bu + v + \partial_a V^I w \\ &= (1-B)^{-1} v + \partial_a V^I (1-B)^{-1} w \\ &= \quad u^0 \quad + \partial_a V^I \quad u' \\ \text{with } u^0 &= (1-B)^{-1} v \text{ and } u' = (1-B)^{-1} w \end{aligned} \tag{26}$$

We now determine $\partial_a V^I$ using the fact that N^I remains constant. Differentiating Eq. (7) leads to

$$\partial_a N^I = \sum_i n_i \sum_{\mu\nu} \left(c_{i\mu} c_{i\nu} \partial_a P_{\mu\nu} + 2 \partial_a c_{i\mu} c_{i\nu} P_{\mu\nu} \right) = 0 \tag{27}$$

which can be expressed with the u matrix

$$\partial_a N^I = \sum_i \sum_{\mu\nu} n_i c_{i\mu} c_{i\nu} \partial_a P_{\mu\nu} + 2 \sum_{ij} n_i u_{ij} \mathscr{P}_{ij} = 0 \tag{28}$$

Using the previous expression for u leads to the following expression for the derivatives of the

Lagrange multiplier

$$\partial_a V^I = -\frac{\sum_i \sum_{\mu\nu} n_i c_{i\mu} c_{i\nu} \partial_a P_{\mu\nu} + 2\sum_{ij} n_i u^0_{ij} \mathscr{P}_{ij}}{2\sum_{ij} n_i u'_{ij} \mathscr{P}_{ij}} \tag{29}$$

$\mathscr{H}$ can now be calculated from Eq. (21), as well as the u matrix from Eq. (19) and finally the derivatives of the coefficients from Eq. (17). The $\mathbf{S}_{IJ}$ derivatives are computed from this MO coefficients derivatives and the derivatives of the AO overlap matrix. For efficiency, the determinant expansions appearing in the calculation of the derivatives were calculated using the Sherman-Morrison formula.[?] A similar approach is applied to the derivatives of the projected overlap matrix $\langle \Phi^I | P^I | \Phi^J \rangle$.

2.5 Variants of the DFTB-VBCI: the HOMO approximation

We will consider the following approximation to the DFTB-VBCI approach: we assume that, in a molecular cluster, the MOs of the different charge localized configurations mostly differ through their Highest Occupied Molecular Orbital (HOMO). The overlaps and projected overlaps between two configurations can be simplified in

$$\mathbf{S}_{IJ} = \langle \Phi^I | \Phi^J \rangle \simeq \langle \phi^I_{\mathrm{HOMO}} | \phi^J_{\mathrm{HOMO}} \rangle \tag{30}$$

$$\langle \Phi^I | P^I | \Phi^J \rangle \simeq N^I \langle \phi^I_{\mathrm{HOMO}} | \phi^J_{\mathrm{HOMO}} \rangle + \langle \phi^I_{\mathrm{HOMO}} | P^I | \phi^J_{\mathrm{HOMO}} \rangle$$

The off-diagonal CI matrix element becomes

$$\begin{aligned} \mathbf{H}_{IJ} &\simeq \frac{1}{2}(\mathbf{H}_I + \mathbf{H}_J) \langle \phi^I_{\mathrm{HOMO}} | \phi^J_{\mathrm{HOMO}} \rangle \\ &- \frac{1}{2}(V^I \langle \phi^I_{\mathrm{HOMO}} | P^I | \phi^J_{\mathrm{HOMO}} \rangle + V^J \langle \phi^I_{\mathrm{HOMO}} | P^J | \phi^J_{\mathrm{HOMO}} \rangle) \end{aligned} \tag{31}$$

The advantage of this approach is to avoid any Slater determinant overlap calculation and only the derivatives of the HOMO coefficients need to be calculated.

3 Applications

We will now apply the DFTB-VBCI method to the treatment of two prototype cationic molecular clusters, namely the benzene dimer and the water dimer.

3.1 Benzene Dimer

Several authors have investigated benzene dimer clusters at high levels of theories. Let us cite for instance MultiReference Configuration Interaction including Single and Double excitations (MR-CISD[40]) and Equation-Of-Motion Coupled-Cluster model with Single and Double substitutions for Ionized systems (EOM-IP-CCSD[41,42]) discussing the relative energies of characteristic isomers, namely the sandwiches (stacked, parallel *x*- and *y*-displaced) and T-shaped configurations (see Figure 1). Both calculations gave the sandwich parallel displaced isomers to be the most stable structures, about 7-8 kcal mol^{-1} lower than the T-shaped. Both approaches can describe in principle correctly the charge resonance states. However MR-CISD may suffer from the lack of size consistence which could explain that the binding energies (12.3 kcal mol^{-1} for the displaced sandwich and 5.4 kcal mol^{-1} for the T-shaped) are significantly smaller than those obtained with EOM-IP-CCSD (20.2 kcal mol^{-1} and 12.4 kcal mol^{-1}) whereas the energy difference between the two isomers is in good agreement (about 7-8 kcal mol^{-1} respectively) **??WARNING cest du MRCPA size consistent??**. The D_{6h} symmetric stacking is another structure of interest which is slightly less stable (about 2 kcal mol^{-1}) than the two sandwich displaced isomers. DFT calculations[43–45] performed with the B3LYP functional give reasonable binding energies for the sandwhich structure (17-19 kcal mol^{-1}) but underestimate the energy difference between the two structures due to an over-stabilization of the T-shaped structure. In the following, we will use the EOM-IP-CCSD[41,42] results as references to benchmark our method as they are the most recent *ab initio* calculations and the corresponding binding energies for the most stable structures around 20 kcal/mol (see Table 1 are in good agreement with the experimental studies providing values in the 15-20 kcal/mol range[44,46–51].

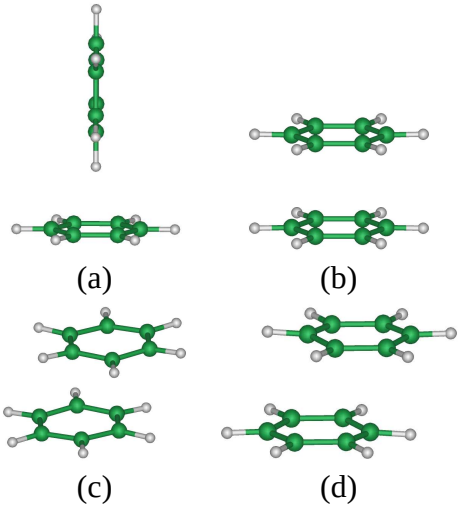

Figure 1: Benzene dimer cations optimized at the DFTB-VBCI level. (a) T-shaped, (b) sandwich stacked, (c) *x*-displaced and (d) *y*-displaced isomers.

Following[41], we call π_g^a and π_g^o the degenerate MO in the neutral benzene molecule. In the ionized monomer, these two levels are degenerate at the neutral geometry but undergo Jahn-Teller distortion leading to an acute angle configuration (ionization from the π_g^a orbital) or an obtuse angle configuration (ionization from the π_g^o orbital). We use the qualitative molecular description of the Dimer Molecular Orbitals Linear Combination from the Fragment Molecular Orbitals (DMO-LCFMO[41]), to describe a benzene dimer, composed of two fragments labelled A and B. In this framework, the constrained state A^+B can be obtained either from removing one electron from the π_g^a or from the π_g^o orbitals of A. Consequently, we need two configurations to describe the constrained form A^+B. In the case of the symmetric D_{6h} sandwich stacked dimer, these two A^+B configurations are degenerate and are built as follows: we use the constrained SCC-DFTB to minimize the electronic energy with an occupation of 1.5 for the two highest occupied MOs (HOMO and HOMO-1) orbitals and 2 for the lower electron energy orbitals. The two A^+B configurations are then built from the obtained MOs as shown on Figure 2. The same procedure is applied to obtain two AB^+ configurations and the CI matrix to be diagonalized is a 4×4 matrix.

In the other isomers (displaced sandwiches and T-shaped), the π_g^a and π_g^o orbitals of each fragments are no longer degenerate and one could in principle calculate the energy of these configura-

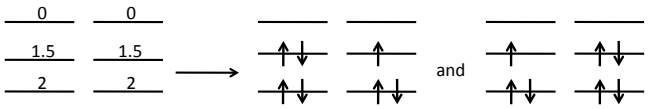

Figure 2: Two electronic configurations (right) obtained from constrained SCC-DFTB calculation with non integer occupation numbers (left).

tions without using fractional occupation numbers. However, we could not obtain a self-consistent solution of the A^+B state (respectively AB^+) with the constrained SCC-DFTB since the π_g^a and π_g^o orbitals on fragment A (respectively on B), although not degenerate remain close in energy. We therefore decided to keep the procedure used for the D_{6h} stacked sandwich isomer filling the HOMO and HOMO-1 orbitals with 1.5 electrons. Although the filling of MO is fixed, these MO relax anyway and are no longer degenerate in the final results, due to the coupling with geometry relaxation.

3.1.1 Sandwich isomer

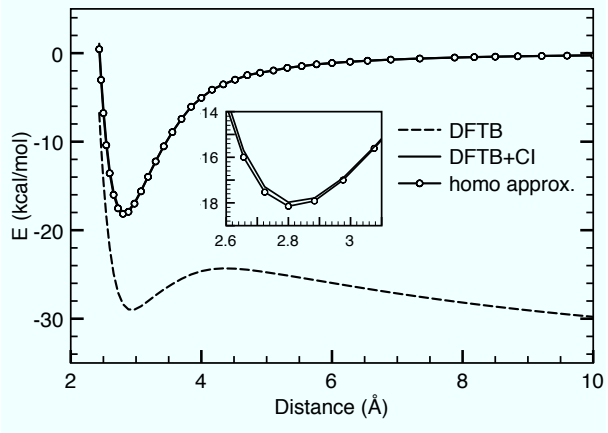

Figure 3: Dissociation potential energy curves of the cationic benzene dimer in the stacked sandwich configuration calculated with SCC-DFTB and DFTB-VBCI approaches.

We first discuss the results obtained for the stacked sandwich in the D_{6h} geometry. Figure 3 represents the energy of the dimer corresponding to dissociation along the *z*-axis, orthogonal to the planes of the monomers. For this example, the fragments are frozen at the monomer neutral geometry). The zero energy reference corresponds to the sum of the separated fragments calculated independently namely $E(C_6H_6^+) + E(C_6H_6)$. The SCC-DFTB dissociation curve reminds the dis-

Table 1: Binding energies of cationic benzene dimer obtained at different levels of theory. The stacked sandwich structure correspond to constrained D_{6h} optimization whereas the other isomers are fully optimized with its respective method. Refs: [a]Pieniazek *et al.*Pieniazek et al.[41] ; [b]Pieniazek *et al.*[42] ; [c]Ibrahim *et al.*[44] ; [d]Itagaki *et al.*[43] ; [e]Kryachko[45] ; [f] Miyoshi *et al.*[40]

	DFTB-VBCI	HOMO Approximation	SCC-DFTB SCC-DFTB	EOM-IP-CCSD EOM-IP-CCSD	DFT DFT	CASSCF+MC CASSCF+MC
Stacked Sandwich	17.70	17.91	29.53	18.34[a]	17.4 [c] - 19.1[d]	
x-displaced	20.90	20.43	29.01	19.58[b]	-	12.3[f]
y-displaced	21.26	20.79	29.21	19.81[b]	16.57[e]	10.9[f]
T-shaped	9.23	16.90	24.68	12.41[b]	15.7 [c]	

sociation curve of H_2^+ calculated with DFT and can be explained as follows. First, the SCC-DFTB energy does not converge to the sum of the energies of the fragments at the dissociation limit. At infinite distance, the charge is equally distributed over the two fragments. As the evolution of the self-interaction error with the number of electrons on a fragment is unfortunately not constant nor linear, we have $2 \times E^{SCC-DFTB}(C_6H_6^{0.5}) \neq E^{\mathrm{SCC-DFTB}}(C_6H_6^+) + E^{\mathrm{SCC-DFTB}}(C_6H_6)$. At shorter distances, the energy increases and a barrier is even observed before reaching the minimum which is here a metastable minimum. The responsible repulsive contribution has a $1/R$ behavior and can be attributed to the artificial repulsion of two half charged fragment, which is a different case of self-interaction than the previous one. Finally, the minimum is much too low in energy (29.5 kcal/mol) as compared to the reference calculations (see Table 1).

As can be seen from Figure 3, the DFTB-VBCI method does not present the wrong behavior pattern of the SCC-DFTB curve. At the dissociation limit, the energy converges to the sum of the energies of the fragments. Actually, in Eq. (12) the overlaps and coupling terms vanish and the energies of the localized configurations are degenerate. These energies are calculated with the electronic density corresponding to one charged and one neutral monomer and not that of two half charged fragments. The Coulombic self-interaction $1/R$ repulsion also disappears with this approach as well as the corresponding barrier. Finally, the binding energy for the stacked sandwich (17.70 kcal/mol) is strongly smaller than the SCC-DFTB one (29.53 kcal/mol) and gives a much better agreement with that of EOM-IP-CCSD calculation at 18.34 kcal/mol.

The dissociation curve obtained applying the HOMO approximation detailed in Section 2.5 is also plotted on Figure 3. It is almost identical to the DFTB-VBCI curve with a binding energy of 17.91 kcal/mol vs 17.70 kcal/mol for the DFTB-VBCI.

3.1.2 T-shaped and displaced sandwich

The T-shaped and displaced sandwiches have been optimized without any geometrical constraint. The binding energies are reported in Table 1. The T-shaped isomer has a binding energy of 9.23 kcal/mol which is slightly smaller than the EOM-IP-CCSD one. Another difference concerns the charge localization. With EOM-IP-CCSD, the charge is mostly localized on the stem fragment (88 %) whereas this localization drops to 56 % with the DFTB-VBCI. A possible explanation for this charge localization discrepancy could be related to lack of stabilization by polarization. In DFTB-VBCI, the benzene π system can be polarized in the direction parallel to the benzene ring. However, due to the reduced basis set used, the polarization of the π system perpendicular to the benzene ring cannot be accounted for. This lack of polarization could be at the origin of the destabilization of the configuration where the charge is carried by the stem fragment, leading to an over-sharing of the charge and an underestimation of the binding energy. Another possibility is the definition of charges of the charge analysis in the *ab initio* calculation (NBO).

At the SCC-DFTB level, the *x*- and *y*- displaced dimers are overstabilized as compared to reference calculations. Similarly to what is observed for the stacked sandwich dimer the DFTB-VBCI approach gives considerably improved binding energies (20.90 and 21.26 kcal/mol) in very good agreements with those of EOM-IP-CCSD (20.14 and 20.18 kcal/mol). These two structures are almost degenerate, the *y*-displaced being slightly more stable. The energy difference is however probably much smaller than the expected accuracy of our approach. These are clearly cases in which quantum vibrational effects should be considered.

Applying the HOMO approximation to the DFTB-VBCI leads to very similar results. The most stable structures are the *x*- and *y*-parallel displaced ones with binding energies which differ by less than 2.5 % from those of DFTB-VBCI. The T-shaped is found to be less stable than the

previous isomers but its binding energy is overestimated compared to reference calculations and DFTB-VBCI, suggesting that the differences between the two configurations can not be reduced to a change in the HOMO.

3.2 Water dimer cation

The potential energy surface of cationic water dimers has been investigated at at hight level of theories CCSD(T)) and EOM-IP-CCSDT[52–55]. The stable structures belong to two families. In the first one, the two water monomers are superimposed in an antisymmetric pattern and the charge is equally distributed over the two units. The second one results from a proton transfer leading to two non-symmetric units $[H_3O - OH]^+$, in which the charge is mostly localized on the H_3O fragment. The structures, found to be minima by Cheng *et al.*[54], have been optimized with DFTB-VBCI method within a conjugated gradient scheme.

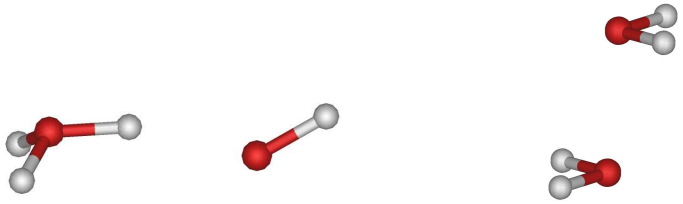

(a) (b)

Figure 4: Water dimer cations optimized at the DFTB-VBCI level. (a) $[H_3O\text{-}OH]^2$ isomer and (b) antisymmetric or $[H_2O\text{-}H_2O]^+$ isomer.

3.2.1 $[H_3O - OH]^+$ structure

Section 3.2 compares the binding energies obtained at the SCC-DFTB level to those resulting from other calculations. For the $[H_3O - OH]^+$, most of the DFT fuctionals (except for the BH&H) give reasonable results compared to CCSD(T) values. Similarly, the binding energy obtained at the SCC-DFTB level, without CI correction is close to that of CCSD(T) (46.3 versus 44.6-45.9).

In this system, the DFTB-VBCI considers the interaction between the configurations where the positive charge is localized either on the H_3O or on the OH subfragments. We started the

Table 2: Binding energies of cationic water dimer obtained at different levels of theory. [a] Lee and KimLee and Kim[55]; [b] Cheng *et al.*Cheng et al.[54]; [c] Barnett and LandmanBarnett and Landman[56]; [d] Sodupe *et al.*[57] MCPF = SCF + electron correlation included with size extensive Modified-Coupled-Pair Functional; [e] Gill and Radom[58]

	AntiSymmetric	H_3O-OH (Cs)	H_3O-OH (C1)
DFTB-VBCI	35.44	42.31	-
HOMO Approx.	35.74	42.33	-
SCC-DFTB	68	46.3	-
GGC	53.73[c]	48.66[c]	-
BLYP	58.4[a]	-	49.3[a]
B3LYP	51.5[a]	-	49.8[a]
MPW1K	42.9[a]	-	49.9[a]
BH&HLYP	41.4 [a]	-	49.9[a]
MP2	40.48[a] / 43.5[e]	50.9[e]	46.47[a]
MP4	41.1[e]	49.9[e]	-
CCSD(T)	39.53[a] / 39.59[b]	46.64[b]	46.70[a] / 46.68[b]
MCPF[d]	36.1	45.9	45.93[d]

optimization from the C_1 global CCSD(T) minimum. The absence of symmetry of this minimum leads to non-degenerate HOMOs. For the two charge-localized configurations. The DFTB-VBCI optimization leads however to a Cs structure. Due to the planar symmetry, degeneracies must be considered in the **detailler .... ??????????????** The weights of the two configurations in the CI approach indicate that the charge is mostly localized (99.9 %) on the H_3O fragment. In CCSD(T) calculations, the charge is localized also strongly localized on this fragment but only at **%??????????????????????**.

We notice that if the DFTB-VBCI minimum (C_s-trans) is different from the C1 minimum obtained with CCSD(T). In CCSD(T), the C_s-trans isomer corresponds to a transition state 0.04 kcal/mol higher in energy than the global C_1 minimum[54] (< 0.2 kcal mol^{-1} for the EOM-IP-CCSD fitted surface of Kamarchik *et al.*[59], and 0.03 kcal/mol at the SCF+MCPF level[57]). Such a small energy difference is far beyond the expected accuracy of the DFTB-VBCI method. The binding energy of C_s-trans isomer is close (42.7 kcal/mol) to that obtained with a simple SCC-DFTB calculation (46.3 kcal/mol). This is due to the fact that the charge is not significantly delocalized between the two fragments and that the SCC-DFTB calculation already attributes most of the

charge to the H_3O fragment. The artificial stabilization by the self-interaction error is therefore less crucial. This also explains why most of the SCC-DFTB functionals give reasonable results for this structure.

3.2.2 Antisymmetric structure

It can be seen from Section 3.2 that, at the CCSD(T) level, the antisymmetric isomer is less stable by 7 kcal/mol than the $[H_3O - OH]^+$ isomer. At the DFT level, the binding energy strongly depends on the choice of the functional. For instance, the $[H_3O - OH]^+$ structure is more stable than $[H_3O - OH]^+$ with MPW1K, BH&H and BH&LYP functionals but it is the opposite with the BLYP, BPW91, HCTH407 and B3LYP functionals. At the SCC-DFTB level, the binding energy of the OO isomer is strongly overestimated (68 versus 39 for CCSD(T)) making this isomer 22 kcal/mol more stable than the $[H_3O - OH]^+$ isomer. The DFTB-VBCI has then a drastic effect, reducing the binding energy to 38 kcal/mol, a value close to the CCSD(T) ones (35-39 kcal/mol). In this isomer, the charge is equally distributed between the two equivalent fragment. The over-stabilization observed at the SCC-DFTB level is attributed to the self-interaction error due to this this strong delocalization and corrected by the DFTB-VBCI approach. Finally, we notice that for both the $[H_3O - OH]^+$ and $[H_2O - H_2O]^+$ isomers, the binding energies obtained with the HOMO approximation are very close to that obtained with the full DFTB-VBCI method.

4 Conclusion

An extended method combining a VBCI-like scheme with the SCC-DFTB has been developed. The method has been implemented together with its analytical gradient to make possible complete optimization, including namely the intra-molecular and inter-molecular degrees of freedom. We have benchmarked this approach on ionized dimers of benzene and water.

In the benzene dimer cation, the self-interaction error is at the origin of an unphysical behavior of the SCC-DFTB dissociation energy curve. It turns to be fully corrected with the DFTB-VBCI as

detailed for the stacked sandwich. This method will allow to perform explorations of potential energy surfaces by molecular dynamics or Monte Carlo sampling with the focus of studying ionized dimers dissociation. The binding energies obtained for different isomers with the DFTB-VBCI compare well with those of high-level calculations as well as experimental data, these standard energies being strongly overestimated with the SCC-DFTB. We however notice that the main error for the DFTB-VBCI binding energy concerns the T-shaped structure which is understabilized by 3 kcal/mol. This may be due to the use of point charges and a possible mistreatment of the multipolar nature of the benzene π system interacting with that of the charged top benzene. Further improvement of the DFTB-VBCI could include such multipolar description of the π system (see for instance[60]) in order to account for this effect but at the price of a larger computational effort to derive the energy gradient.

The second benchmark system is the ionized water dimer. The two main isomers strongly differ by a proton transfer. The binding energy of $[H_3O-OH]^+$ isomers calculated at the DFT level with several functionals are in good agreement with reference calculations. This is also the case with SCC-DFTB and DFTB-VBCI due the localization of the charge on the H_3O subfragment reducing the multiconfigurational nature of the wavefunction and the self-interaction error in standard DFT based calculations. On the opposite, in the $[H_2O-H_2O]^+$ isomer the charge is equally carried by the two fragments and the binding energies obtained at DFT level strongly differ depending on the choice of the functional. With SCC-DFTB, this structure is overstabilized and becomes artificially the most stable one. This effect is corrected with the DFTB-VBCI approach which gives a binding energy close to that of high level of calculations.

Taking advantage of the SCC-DFTB in terms of computational efficiency, the DFTB-VBCI will allow to deal with systems larger than dimers. In our previous study, DFTB-VBCI has been used to characterize binding energies, ionization potentials as well as charge localization in stacked coronene clusters with frozen intramolecular geometries and equal spacings between the planes of the units[35]. This work was however performed before the development of analytical gradients and it will be of interest to characterize the effects of intra- and inter-molecular relaxation in these

clusters. It is known that in rare gas clusters He_n^+, Ne_n^+, Ar_n^+, Kr_n^+ and Xe_n^+, the hole tends to delocalize on few units (from 2 to 4, depending the rare gas) and that the other atoms tend to organize in crowns around a linear core. It will be intersesting to understand how the internal degrees of freedom, the molecular extension and shape influence the size of the core unit and the organization of the whole cluster.

- Pour l’eau : Decrire notre choix de remplissage electronique H3O-OH
- Pour l’eau : dans la litterature la valeur de la charge sur H3O donnee en DOHF et excitation seulement ?
- Pour le sandwich stacked la courbe ne correspond pas aux valeurs du tableau !!!! refaire avec la meme dispersion
- parler des comparaison avec la SIC DFT (pienazcek)
- pour le water H3O-OH charge localization Cheng donne les valeurs ROHF ....
- faire le calcul H3O-OH avec le 0.5 pr le OH
- mettre 1 ref ancienne pour le coupled perurbed equations
- formule du homo a approx
- figure 3 ecrire SCC-DFTB
- ecrire les gradient dans la conclusion
- gradient complet + colle a l’experience

References

(1) Wu, Q.; Cheng, S.-L.; Van Voorhis, T. *J. Chem. Phys.* **2007**, *127*, 164119.

(2) Zhao, Y.; Schultz, N. E.; Truhlar, D. G. *J. Chem. Phys.* **2005**, *123*, 161103–4.

(3) Dion, M.; Rydberg, H.; Schröder, E.; Langreth, D. C.; Lundqvist, B. I. *Phys. Rev. Lett.* **2004**, *92*, 246401.

(4) Sato, T.; Tsuneda, T.; Hirao, K. *J. Chem. Phys.* **2005**, *123*, 104307–10.

(5) Sato, T.; Tsuneda, T.; Hirao, K. *J. Chem. Phys.* **2007**, *126*, 234114–12.

(6) Langreth, D. C.; Dion, M.; Rydberg, H.; Schroder, E.; Hyldgaard, P.; Lundqvist, B. I. *Int. J. Quant. Chem.* **2005**, *101*, 599–610.

(7) Chakarova-Kack, S. D.; Schroder, E.; Lundqvist, B. I.; Langreth, D. C. *Phys. Rev. Lett.* **2006**, *96*, 146107–4.

(8) Thonhauser, T.; Cooper, V. R.; Li, S.; Puzder, A.; Hyldgaard, P.; Langreth, D. C. *Phys. Rev.B* **2007**, *76*, 125112–11.

(9) von Lilienfeld, O. A.; Tavernelli, I.; Rothlisberger, U.; Sebastiani, D. *Phys. Rev. Lett.* **2004**, *93*, 153004.

(10) Zhao, Y.; Truhlar, D. G. *J. Phys. Chem.A* **2004**, *108*, 6908–6918.

(11) Lewis, J. P.; Sankey, O. F. *Biophys. J.* **1995**, *69*, 1068.

(12) Meijer, E. J.; Sprik, M. *J. Chem. Phys.* **1996**, *105*, 8684–8689.

(13) Gianturco, F. A.; Paesani, F.; Laranjeira, M. F.; Vassilenko, V.; Cunha, M. A. *J. Chem. Phys.* **1999**, *110*, 7832–7845.

(14) Elstner, M.; Hobza, P.; Frauenheim, T.; Suhai, S.; Kaxiras, E. *J. Chem. Phys.* **2001**, *114*, 5149–5155.

(15) Wu, Q.; Yang, W. *J. Chem. Phys.* **2002**, *116*, 515–524.

(16) Zimmerli, U.; Parrinello, M.; Koumoutsakos, P. *J. Chem. Phys.* **2004**, *120*, 2693–2699.

(17) Grimme, S. *J. Comput. Chem.* **2004**, *25*, 1463.

(18) Goursot, A.; Mineva, T.; Kevorkyants, R.; Talbi, D. *J. Chem. Theor. Comput.* **2007**, *3*, 755–763.

(19) Savin, A. *Recent developments and applications of modern Density Functional Theory*; J. Seminario, Elsevier, Amsterdam, 1996.

(20) Leininger, T.; Stoll, H.; Werner, H.-J.; Savin, A. *Chem. Phys. Lett.* **1997**, *275*, 151.

(21) Goll, E.; Werner, H.-J.; Stoll, H. *Phys. Chem. Chem. Phys.* **2005**, *7*, 3917.

(22) Goll, E.; Werner, H. J.; Stoll, H. *Chem. Phys.* **2008**, *346*, 257.

(23) Heitler, W.; London, F. *Z. Physik* **1927**, *44*, 455.

(24) Pauling, L. *The nature of the Chemical Bond*; Cornell University Press, New York, 1939.

(25) Murrel, J.-N.; Tedder, S.-F. *The Chemical Bond*; John Wiley & Sons, 1985.

(26) Shaik, S. S.; Hiberty, P. C. *A Chemist's Guide to Valence Bond Theory*; New Jersey: Wiley-Interscience, 2008.

(27) Bouvier, B.; Brenner, V.; Millié, P.; Soudan, J.-M. *J. Phys. Chem.A* **2002**, *106*, 10326.

(28) Wu, Q.; Van Voorhis, T. *J. Chem. Theor. Comput.* **2006**, *2*, 765–774.

(29) Wu, Q.; Van Voorhis, T. *J. Chem. Phys.* **2006**, *125*, 164105.

(30) Van Voorhis, T.; Kowalczyk, T.; Kaduk, B.; Wang, L.-P.; Cheng, C.-L.; Wu, Q. *Annual Review of Physical Chemistry* **2010**, *61*, 149–170.

(31) Porezag, D.; Frauenheim, T.; Köhler, T.; Seifert, G.; Kaschner, R. *Phys. Rev.B* **1995**, *51*, 12947.

(32) Seifert, G.; Porezag, D.; Frauenheim, T. *Int. J. Quant. Chem.* **1996**, *58*, 185.

(33) Elstner, M.; Porezag, D.; Jungnickel, G.; Elsner, J.; Haugk, M.; Frauenheim, T.; Suhai, S.; Seifert, G. *Phys. Rev.B* **1998**, *58*, 7260.

(34) Oliveira, A.; Seifert, G.; Heine, T.; duarte, H. *J. Braz. Chem. Soc.* **2009**, *20*, 1193.

(35) Rapacioli, M.; Spiegelman, F. *Eur. Phys. J. D* **2009**, *52*, 55.

(36) Wu, Q.; Van Voorhis, T. *Physical Review A* **2005**, *72*, year.

(37) Ryckaert, J.; Cicotti, G.; Berendsen, H. *J. Comput. Phys.* **1977**, *23*, 327.

(38) Rapacioli, M.; Barthel, R.; Heine, T.; Seifert, G. *J. Chem. Phys.* **2007**, *126*, 124103.

(39) Wolff, S. *Int. J. Quant. Chem.* **2005**, *104*, 645–659.

(40) Miyoshi, E.; Yamamoto, N.; Sekiya, M.; Tanaka, K. *Mol. Phys.* **2003**, *101*, 227–232.

(41) Pieniazek, P. A.; Krylov, A. I.; Bradforth, S. E. *J. Chem. Phys.* **2007**, *127*, year.

(42) Pieniazek, P. A.; Bradforth, S. E.; Krylov, A. I. *J. Chem. Phys.* **2008**, *129*, year.

(43) Itagaki, Y.; Benetis, N. P.; Kadam, R. M.; Lund, A. *Phys. Chem. Chem. Phys.* **2000**, *2*, 2683–2689.

(44) Ibrahim, Y.; Alsharaeh, E.; Rusyniak, M.; Watson, S.; Mautner, M. M. N.; El-Shall, M. S. *Chem. Phys. Lett.* **2003**, *380*, 21–28.

(45) Kryachko, E. S. *Int. J. Quant. Chem.* **2007**, *107*, 2741–2755.

(46) Field, F. H.; Hamlet, P.; Libby, W. F. *J. Am. Chem. Soc.* **1969**, *91*, 2839–2842.

(47) Grover, J. R.; Walters, E. A.; Hui, E. T. *J. Phys. Chem.* **1987**, *91*, 3233–3237.

(48) Krause, H.; Ernstberger, B.; Neusser, H. J. *Chem. Phys. Lett.* **1991**, *184*, 411–417.

(49) Meot-Ner, M.; Hamlet, P.; Hunter, E. P.; Field, F. H. *J. Am. Chem. Soc.* **1978**, *100*, 5466–5471.

(50) Hiraoka, K.; Fujimaki, S.; Aruga, K.; Yamabe, S. *J. Chem. Phys.* **1991**, *95*, 8413–8418.

(51) Rusyniak, M.; Ibrahim, Y.; Alsharaeh, E.; Meot-Ner(Mautner), M.; El-Shall, M. *J. Phys. Chem.A* **2003**, *107*, 7656–7666.

(52) Pieniazek, P. A.; VandeVondele, J.; Jungwirth, P.; Krylov, A. I.; Bradforth, S. E. *J. Phys. Chem.A* **2008**, *112*, 6159–6170.

(53) Periyasamy, G.; Levine, R. D.; Remacle, F. *Chem. Phys.* **2009**, *366*, 129–138.

(54) Cheng, Q.; Evangelista, F. A.; Simmonett, A. C.; Yamaguchi, Y.; Schaefer, H. F. *J. Phys. Chem.A* **2009**, *113*, 13779–13789.

(55) Lee, H. M.; Kim, K. S. *Journal of Chemical Theory and Computation* **2009**, *5*, 976–981.

(56) Barnett, R. N.; Landman, U. *J. Phys. Chem.* **1995**, *99*, 17305–17310.

(57) Sodupe, M.; Oliva, A.; Bertran, J. *J. Am. Chem. Soc.* **1994**, *116*, 8249–8258.

(58) Gill, P. M. W.; Radom, L. *J. Am. Chem. Soc.* **1988**, *110*, 4931–4941.

(59) Kamarchik, E.; Kostko, O.; Bowman, J. M.; Ahmed, M.; Krylov, A. I. *J. Chem. Phys.* **2010**, *132*, 194311.

(60) Piquemal, J.-P.; Gresh, N.; Giessner-Prettre, C. *J. Phys. Chem.A* **2003**, *107*, 10353–10359.